Nuclear Inst. and Methods in Physics Research, A 886 (2018) 36–39

Contents lists available at ScienceDirect

Nuclear Inst. and Methods in Physics Research, A

journal homepage: www.elsevier.com/locate/nima

Performance of μ-RWELL detector *vs* resistivity of the resistive stage

G. Bencivenni [a], R. De Oliveira [b], G. Felici [a], M. Gatta [a], G. Morello [a,*], A. Ochi [c], M. Poli Lener [a], E. Tskhadadze [a,d]

[a] *Laboratori Nazionali di Frascati dell'INFN, Frascati, Italy*
[b] *CERN, Geneva, Switzerland*
[c] *Kobe University, Kobe, Japan*
[d] *JINR, Dubna, Russia*

ARTICLE INFO

Keywords:
Micro-Resistive WELL
MPGD
Gaseous detectors

ABSTRACT

The μ-RWELL is a compact spark-protected single amplification stage Micro-Pattern-Gaseous-Detector (MPGD). The detector amplification stage is realized with a polyimide structure, micro-patterned with a dense matrix of blind-holes, integrated into the readout structure. The anode is formed by a thin Diamond Like Carbon (DLC) resistive layer separated by an insulating glue layer from the readout strips. The introduction of the resistive layer strongly suppressing the transition from streamer to spark gives the possibility to achieve large gains (> 10^4), without significantly affecting the capability to be efficiently operated in high particle fluxes. In this work we present the results of a systematic study of the μ-RWELL performance as a function of the DLC resistivity. The tests have been performed either with collimated 5.9 keV X-rays or with pion and muon beams at the SPS Secondary Beamline H4 and H8 at CERN.

1. Introduction

The μ-RWELL has been introduced as a thin, simple and robust detector for very large area applications requiring the operation in harsh radiation environment [1]. The detector, as sketched in Fig. 1, is composed of two main components: the cathode and the μ-RWELL Printed Circuit Board (PCB), the core of the detector. The μ-RWELL-PCB, a multi-layer circuit produced with standard photo-lithography technology, is composed of three different elements: a suitably patterned Kapton® foil that acts as amplification stage of the detector; a grounded resistive layer as discharge limitation stage; a standard segmented copper electrode on a printed circuit board for readout purposes.

MPGDs, due to their typical micrometric distance of the electrodes, generally suffer from discharge occurrence that can eventually damage or destroy the detector as well as the associated front-end electronics or lead to dead time and detection inefficiencies. In the μ-RWELL, following the experiences with the MicroMegas [2] and the Micro Gap Resistive Plate Chambers (MGRPC) [3], this problem has been substantially solved with the introduction of a resistive layer on the bottom side of the Kapton® foil. The discharge suppression mechanism is the same of the resistive electrode used in the RPCs [4–6]: the streamer generated in the gas gap inside the amplification volume, inducing a large current through the resistive layer, generates a local drop of the amplifying voltage with an effective quenching of the multiplication process in the gas. This mechanism strongly suppressing the discharge amplitude (down to few tens of nano-ampere [1]) gives the possibility to achieve large gains with only one amplification stage.

A drawback, strictly correlated with the Ohmic behavior of the detector is the reduced capability to be efficiently operated in high particle fluxes [1].

Finally the implementation of the resistive layer affects the charge spread on the readout electrodes (Fig. 2): the charge collected on the resistive stage is dispersed with a time constant [7]

$$\tau = \rho c = \rho \frac{\epsilon_0 \epsilon_r}{t}$$

being ρ the surface resistivity, c the capacitance per unit area and t the distance between the resistive layer and the readout plane. Two different schemes have been studied for the resistive stage: the simplest layout, based on a homogeneous resistive layer, grounded at the edges (2D-current evacuation), in the following referred to as single-resistive layer, has been designed for low-rate applications (Fig. 3); a more sophisticated one, based on a double-resistive layer with a proper density of vias between the two layers with the grounding done by

* Corresponding author.
E-mail address: morello@lnf.infn.it (G. Morello).

https://doi.org/10.1016/j.nima.2017.12.037
Received 16 May 2017; Received in revised form 26 October 2017; Accepted 11 December 2017
Available online 24 December 2017

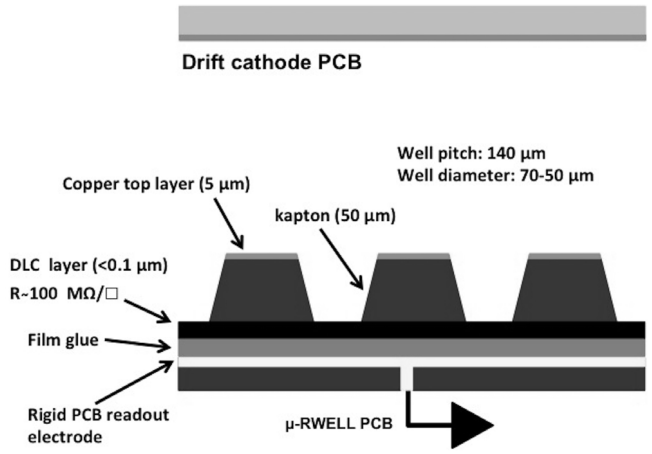

Fig. 1. Sketch of the μ-Resistive WELL.

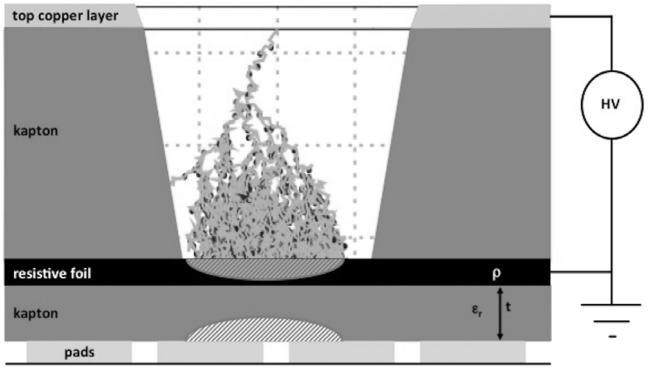

Fig. 2. Sketch of the electronic avalanche in a μ-RWELL: the charge collected on the resistive layer induces the signal on the readout electrodes.

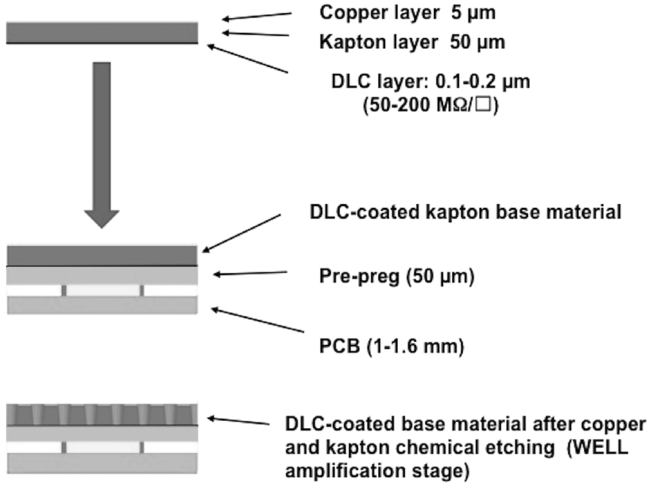

Fig. 3. Single resistive layer scheme for low rate operation.

means of the readout electrodes (3D-current evacuation) is under study for high-rate purposes. In this paper we focus on the single-resistive layout.

2. Detectors description

The three prototypes used in this work are single-resistive layer detectors with DLC layer resistivity of 12/80/880 MΩ/□. One of the major difference of such detectors with respect to the first version of the μ-RWELL [1] is that the copper dots, patterned on the bottom side of the foil in correspondence of each WELL structure, have been removed thanks to the use of the DLC that ensures a high chemical and mechanical stability. Moreover a global irradiation test at the GIF++ CERN facility is in progress to study possible aging effects on the DLC. All prototypes under study were equipped with a readout patterned with a 400 μm pitch strips. In Table 1 the characteristics of the prototypes are reported.

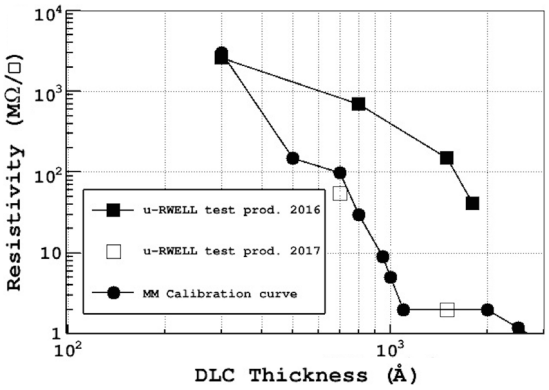

Fig. 4. Resistivity as a function of the sputtered DLC thickness for different sputtering batches.

2.1. DLC sputtering

Sputtering is commonly used to deposit thin protective films on a substrate. For the production of our detectors, a large industrial sputtering chamber in Be-Sputter Co., Ltd. (Japan) has been used. The carbon is sputtered on the Kapton® foil as an amorphous DLC using a pure graphite target. The resistivity dependence as a function of the DLC thickness for different sputtering batches is shown in Fig. 4. The MM calibration curve has been obtained by sputtering the DLC on a brand-new Kapton® foil [8].

The two open square markers, referring to the μ-RWELL 2017 test production, for which the base material has been pre-dried in an oven (200° for approximately 2 h), match the MM calibration curve. The dropping curve refers to the 2016 test production. The different trend for the two curves is assumed to be related with the humidity trapped by the Kapton® before the sputtering process.

3. Laboratory tests

The characterization of the detectors is performed with collimated 5.9 keV photons generated by an X-ray gun (PW2217/20 Philips). The gas gain of the detectors has been measured in current mode: the current drawn at a given potential through the resistive layer has been normalized to the ionization current, recorded operating the detector at unitary gain (very low voltage). The gain has been then plotted as a function of the amplification potential. As shown in Fig. 5, the gas gain of the various detectors, measured for the Ar:i-C_4H_{10} (90:10 vol%) gas mixture, and parametrized as $G = e^{(\alpha\Delta V - \beta)}$, is typically ≥ 10000, being stopped when current instabilities (not discharges) are observed:[1] the largest gain is generally reached by the detector with highest resistivity. The rate capability has been measured at the gain G~4000, well above the knee of the efficiency plateau (Section 4). The X-ray gun can provide photon-converted signal rate ranging from 1 kHz up to approximately 300 kHz. The equivalent flux is obtained by dividing the measured rate

[1] As shown in Fig. 9 of [1].

Table 1
Detectors characteristics.

Detector characteristics	Detector n.1	Detector n.2	Detector n.3
DLC resistivity MΩ/□	12	80	880
Hole pitch (μm)	140	100	100
External/internal hole diameter (μm)	70/50	55/50	70/30
Active area (mm^2)	100 × 100	50 × 50	50 × 50
Readout strip pitch (mm)	0.4	0.4	0.4

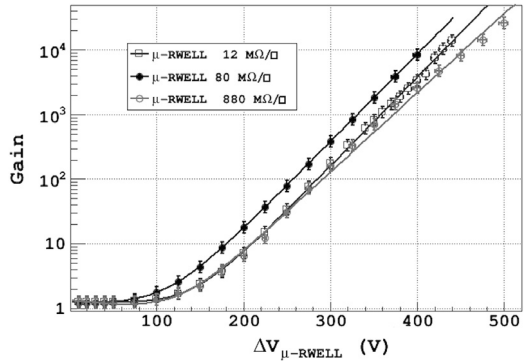

Fig. 5. Measured gain for the three detectors at STP.

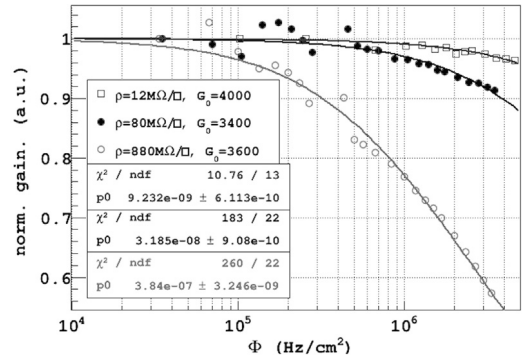

Fig. 6. Normalized gain for 12 MΩ/□ (open squares), 80 MΩ/□ (full circles) and 880 MΩ/□ (open circles).

by the irradiated area, given by the collimator surface [2] and for each flux we have plotted the ratio of the measured gain to the nominal gain at low rate (Fig. 6). The points are fitted with the function

$$\frac{G}{G_0} = \frac{-1+\sqrt{4p_0\Phi}}{2p_0\Phi} \quad (1)$$

introduced and derived in the appendix A of [1]. Reverting the Eq. (1) we can obtain the value of the flux at a given normalized gain drop of 3%, representing our definition of the detector rate capability. As expected, the gain decrease is correlated with the voltage drop due to current through the resistive layer: larger the DLC layer resistivity, the lower is the rate capability, ranging, for local irradiation, from few tens of kHz/cm^2 up to few MHz/cm^2, even though in case of global irradiation and large area detector we expect a rate capability much lower than the values measured with collimated X-rays.

A more realistic measurement of the rate capability has been obtained irradiating with a pion beam, with a spot area of approximately 3 × 3 cm^2 (FWHM), two different zones of a further single-resistive layer detector (∼ 1.2 × 0.5 m^2) with a ∼ 70 MΩ/□ resistivity. The result reported in Fig. 7 shows that the two zones can be operated up to 35 kHz/cm^2 without appreciable gain losses.

[2] We performed a local irradiation of the detector with a 2.5 mm diameter brass collimator.

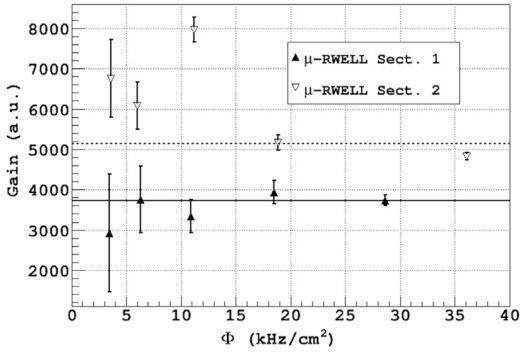

Fig. 7. Rate capability as a function of the H8-SPS CERN pion beam flux for two different zones of a large area single layer μ-RWELL. The two zones have been operated at different gains as shown by the fit lines.

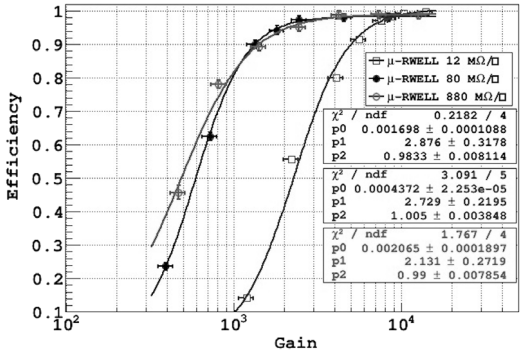

Fig. 8. Tracking efficiency as a function of the gain for the three detectors.

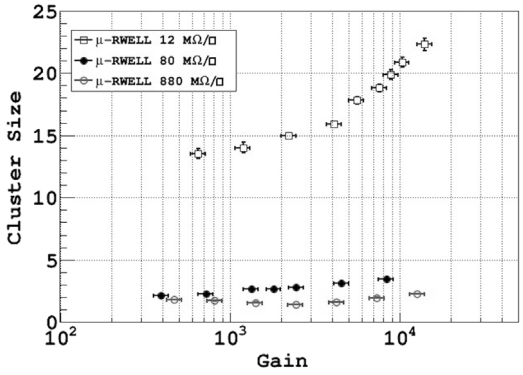

Fig. 9. Strip cluster size (average number of contiguous fired strip per track) as a function of the gain for the three detectors.

4. Beam test results

The tracking performance of the three detectors has been investigated at the H4-SPS CERN muon beam. The setup has been composed of four trigger scintillators (two read-out with Silicone Photomultipliers and two with Photomultiplier tubes) and two tracking stations

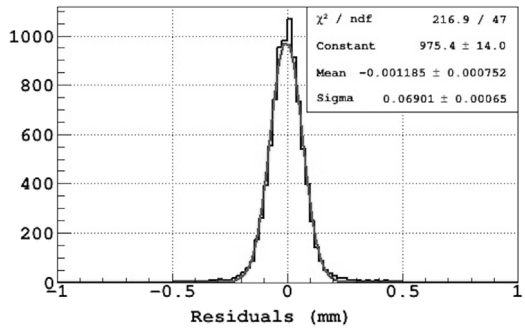

Fig. 10. Residuals distribution for orthogonal tracks impinging the 80 MΩ/□ prototype.

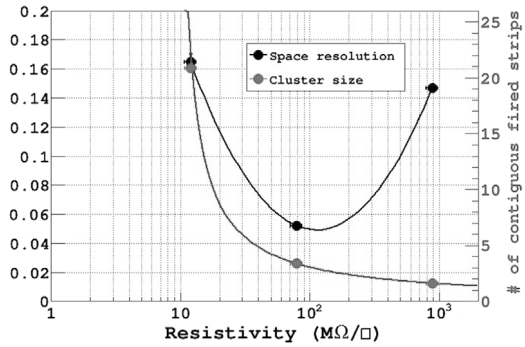

Fig. 11. Space resolution and strip cluster size as a function of the DLC resistivity. The detector has been operated at gains ensuring full efficiency.

each consisting of two triple-GEM detectors with two-dimensional strip readout. All gaseous detectors have been operated in Ar:i-C_4H_{10} (90:10 vol%) at atmospheric pressure and were read-out with APV front-end cards [9], interfaced by the Scalable Readout System [10]. The APV chip, supplying analog output signals, allows the study of the detector tracking performance based on the charge centroid method.

In Fig. 8 the tracking efficiency of the detectors is reported as a function of the gain:[3] all detectors achieve a tracking efficiency above 98%. The shift of the efficiency curve of the 12 MΩ/□ prototype with respect to the others is correlated with the large charge spread occurring at low DLC resistivity (Fig. 9): the charge dispersion on the readout strips increases, the signal collected by each pre-amplifier channel decreases thus requiring a higher gain to reach the full detector efficiency.

The narrower residuals distribution, Fig. 10, for the 80 MΩ/□ prototype has been obtained at a gain G∼ 4000 with orthogonal tracks showing a standard deviation of 69 ± 1 μm. Subtracting the contribution of the external trackers (σ_{fit} = 47 ± 5 μm), evaluated from the average width of their residuals,[4] a spatial resolution of 52 ± 6 μm has been derived.

Eventually, as reported in Fig. 11, the space resolution depends on the resistivity of the DLC, showing a minimum around a surface resistivity of about 100–200 MΩ/□. At low surface resistivity the charge distribution loses the typical Gaussian shape and consequently the σ becomes larger. At high surface resistivity the charge dispersion is so negligible (the strip cluster size being close to 1) that the charge centroid method becomes no more effective and the σ approaches the limit of pitch/$\sqrt{12}$.

5. Conclusions

In this work we have discussed the results of a systematic study of μ-RWELL performance as a function of the DLC resistivity. All the detectors, realized with the single-resistive layout, exhibit a gas gain up to and above 10^4 with Ar:i-C_4H_{10} (90:10 vol%) gas mixture. A rate capability up to 35 kHz/cm^2 has been measured and a spatial resolution better than 100 μm has been obtained, showing a minimum between 100 and 200 MΩ/□.

References

[1] G. Bencivenni, et al., The micro-Resistive WELL detector: A compact spark-protected single amplification-stage MPGD, J. Instrum. 10 (2015) P02008.
[2] T. Alexopoulos, et al., A spark-resistant bulk-micromegas chamber for high-rate applications, Nucl. Instrum. Methods A 640 (2011) 110–118.
[3] A. Di Mauro, et al., Development of innovative micropattern gaseous detectors woth resistive electrodes and first results of their applications, arXiv:07060102pdf.
[4] Y. Pestov, et al., A spark counter with large area, Nucl. Instrum. Methods 93 (1971) 269.
[5] R. Santonico, R. Cardarelli, Development of resistive plate counters, Nucl. Instrum. Methods A 377 (1981) 187.
[6] M. Anelli, et al., Glass electrode spark counters, Nucl. Instrum. Methods A 300 (1991) 572.
[7] M.S. Dixit, et al., Simulating the charge dispersion phenomena in micro pattern gas detectors with a resistive anode, Nucl. Instrum. Methods A 566 (2006) 281.
[8] A. Ochi, et al., Carbon sputtering Technology for MPDG detectors, Proceeding of Science (TIP2014),351.
[9] M. Raymond, et al., The APV25 0.25m CMOS readout chip for the CMS tracker, IEEE Nucl. Sci. Symp. Conf. Rec. 2 (2000) 9/113.
[10] S. Martoiu, et al., Development of the scalable readout system for micro-pattern gas detectors and other applications, J. Instrum. 8 (2013) C03015.

[3] The tracking efficiency is defined as the ratio of the *good cluster of fired strips in the* μ-RWELL to the *total number of good tracks (reconstructed by the four external trackers)*; the good clusters are chosen to be inside ±3σ of the residuals distribution.

[4] Defined as $x_{fit} - x_{meas}$, where x_{fit} is the intersection of the track, reconstructed with three detectors, with the excluded one and x_{meas} is its cluster centroid coordinate.